Available online at BCREC Website: http://bcrec.undip.ac.id

Bulletin of Chemical Reaction Engineering & Catalysis, 8 (2), 2013, 137-144

Research Article

Application of Cement Clinker as Ni-Catalyst Support for Glycerol Dry Reforming

Hua Chyn Lee, Kah Weng Siew, Jolius Gimbun, Chin Kui Cheng *

Faculty of Chemical & Natural Resources Engineering, Universiti Malaysia Pahang, Lebuhraya Tun Razak, 26300 Gambang Kuantan, Pahang, Malaysia

Received: 30th May 2013; Revised: 27th August 2013; Accepted: 11st September 2013

Abstract

The increase in biodiesel production inevitably yield plethora of glycerol. Therefore, glycerol has been touted as the most promising source for bio-syngas (mixture of H_2 and CO) production. Significantly, coking on nickel-based catalysts has been identified as a major deactivation factor in reforming technology. Indeed, coke-resistant catalyst development is essential to enhance syngas production. The current work develops cement clinker (comprised of 62.0% calcium oxide)-supported nickel catalyst (with metal loadings of 5, 10, 15 and 20 wt%) for glycerol dry reforming (CO_2). Physicochemical characterization of the catalysts was performed using XRD, XRF, BET, TGA and FESEM-EDS techniques. Subsequently, reaction studies were conducted in a 7-mm ID fixed-bed stainless steel reactor at 1023 K with various CO_2 partial pressures at constant weight-hourly space velocity (WHSV) of 7.2×104 ml g_{cat}^{-1} h^{-1}. Gas compositions were determined using Agilent 3000 micro-gas chromatography (GC) and Lancom III gas analyzer. Results obtained showed an increment of BET surface area up to 32-fold with Ni loading which was corroborated by FESEM images. Syngas (H_2 and CO) ratios of less than 2 were being produced at 1023 K. A closer scrutiny to the transient profile revealed that the presence of CO_2 higher or lower than CGR 1:1 promotes the Boudouard reaction.

Keywords: Bio-syngas; cement clinker; glycerol; dry reforming

How to Cite: Lee, H.C., Siew, K.W., Cheng, C.K. (2013). Application of Cement Clinker as Ni-Catalyst Support for Glycerol Dry Reforming. *Bulletin of Chemical Reaction Engineering & Catalysis*, 8 (2): 137-144. (doi:10.9767/bcrec.8.2.5023.137-144)

Permalink/DOI: http://dx.doi.org/10.9767/bcrec.8.2.5023.137-144

1. Introduction

Post year 2008, in the aftermath of global energy crisis sparked by the sudden surge in the price of petroleum fuel, the search for renewable and sustainable energy source has become imperative. For countries with meager proven petroleum reserves such as Malaysia, a moratorium on petroleum oil production could spell a disaster to the economy; hence energy security in the context of leveraging on the country's biodiversity is clearly the only way out from the energy malaise. Significantly, syngas (H_2 and CO) production from glycerol bio-waste (10 wt% of crude glycerol per kg of biodiesel from the transesterification process) has been touted as one of the most promising route in achieving sustainable energy requirement. Indeed, the H_2 combustion value is 122 kJ g^{-1}, which is 2.75-fold of hydrocarbon fuels [1]. In theory, 1 mole of glycerol can decompose to 3 mol of CO and 4 mol

* Corresponding Author.
E-mail: chinkui@ump.edu.my (C.K. Cheng)
Tel: +60-9-5492896, Fax: +60-9-5492889

of H_2 (cf. Equation (1)).

$$C_3H_8O_3\,(g) \leftrightarrow 3CO\,(g) + 4H_2\,(g) \quad (1)$$

Production of syngas from glycerol steam reforming has been studied. However, it does not yield favourable H_2:CO ratio for Fisher-Tropsch (FT) synthesis. Besides, it also emits CO_2 (cf. Equation (2)).

$$C_3H_8O_3\,(g) + 3H_2O\,(g) \leftrightarrow 3CO_2\,(g) + 7H_2\,(g) \quad (2)$$

In particular, glycerol dry reforming as shown in Equation (3) is a new area and no prior works have been published on it. Theoretical consideration alone indicates that it is more viable for syngas production intended for FT synthesis as well as utilizing the greenhouse gas, CO_2. Wang *et al.* [2] from their thermodynamic analysis reported that glycerol dry reforming is able to produce 6.4 moles of syngas per mole of glycerol.

$$C_3H_8O_3(g) + CO_2(g) \leftrightarrow 4CO(g) + 3H_2(g) + H_2O(g) \quad (3)$$

In reforming technologies, Ni catalyst has been widely used due to its availability and low costs compared to noble metals such as Rh, Pt and Pd [3-5]. Nonetheless, the main drawback associated with Ni is severe carbon deposition (coking). Significantly, coking onto the catalysts can be reduced by the addition of strong Lewis base oxide such as CaO [6-10] previously reported that cement clinker contains 63.28% and 63.17% CaO, respectively. Importantly, it is an abundant source from cement industry in Malaysia. Endowed by thermal stability, cement clinker hence offers great potential as suitable support for Ni catalyst.

The current work serves to characterize the synthesized cement clinker-supported nickel catalysts using spectroscopic analysis and also to investigate the activity of glycerol dry reforming over the cement clinker-supported Ni catalyst with the aims of producing syngas mixture suitable for FT synthesis and enhancing catalytic stability through carbon lay down reduction.

2. Materials and Methods

2.1. Materials and Catalyst preparation

Cement clinker (CC) was obtained from the Pahang Cement Sdn. Bhd. after the cement kiln which undergone calcination at 1673 to 1723 K. All the chemicals such as nickel (II) nitrate hexahydrate ($Ni(NO_3)_2{\cdot}6H_2O$) and pure glycerol were analytical grade purchased from Sigma-Aldrich. Catalysts were prepared via wet-impregnation of CC with 5 wt%, 10 wt%, 15 wt% and 20 wt % nickel (Ni)-metal respectively using $Ni(NO_3)_2.6H_2O$ solution prepared from 50 ml ultrapure water (Milipore Elix 5-UV) as precursors. The slurry was then stirred for 3 h at room temperature before oven-dried at 403 K for 24 h. Subsequently, it was calcined at 1073 K for 6 h. Post-calcination, the catalysts were ground and sieved to the size < 200 µm for reaction studies.

2.2. Characterization of The Catalysts

The freshly-calcined catalysts were subjected to a series of characterization, viz. thermogravimetric analysis (TGA), x-ray fluorescence (XRF), x-ray diffraction (XRD), field emission scanning electron microscopy-energy dispersive x-ray spectrometry (FESEM-EDS) and also specific surface area measurement by liquid N_2 adsorption analysis. The XRD measurement employed radiation, λ= 1.5418 Å at 30 kV and 15 mA, in 2θ from 10^o to 80^o with a step size of 0.02^o and step time of 1 s. The crystalline size of the catalysts was determined from the Scherrer equation, $d=0.94\lambda/(\beta d\cos\theta)$, where d is the crystallite size, λ is the wavelength of the radiation, βd is the full-width at half maximum (FWHM) of the diffraction peak and θ is the half of the diffraction angle. The surface structure of the catalysts was captured by FESEM unit JOEL/JSM-7800F model at 3 kV with ×10,000 magnification. Specific surface area was determined by BET model. The catalysts were degassed overnight at 573 K prior to specific surface area measurement at 77 K. The cumulative pore volumes of the catalysts were determined by using Barrett-Joyner-Halenda (BJH) analysis. The chemical composition of the catalysts was determined by both EDS and XRF. TGA analysis was performed to obtain the phase transformation of the catalyst in N2 atmosphere up to 1173 K employing the ramping rates of 10 K min^{-1}.

2.3. Catalyst Testing

Figure 1 shows the experimental rig for the catalyst testing. The catalytic evaluation was carried out by placing 0.10 g of catalyst into the stainless steel 316 fixed-bed reactor (ID: 7 mm) supported by two layers of quartz wool. The catalyst was reduced by 50% H_2/Ar gas (50 ml min-1 STP) for 2 h and held at 1073 K. Glycerol was pumped into the reactor by HPLC pump while the flowrate of carrier gas (as diluent) was controlled using flowmeter controller. CO_2 to glycerol ratio (CGR) was adjusted to determine the partial pressure of the reactants at constant weight-hourly space velocity (WHSV) of 7.2×10^4 ml g_{cat}^{-1} h^{-1}. The reaction temperature was set at 1023 K and ex-

periments were repeated at temperatures between 973 and 923 K respectively. The composition of produced syngas was determined using online Agilent 3000 micro-gas chromatography (GC) with TCD column, Backflush Molecular Sieve 5A (10 m × 0.32 mm) and Plot U column (3 m × 0.32 mm) and Lancom III gas analyzer.

2.4 Power Law Model

Power law equation (cf. Equation (4)) was being used to approximate the kinetics of the glycerol dry reforming reactions and also its rate exponential.

$$r = kP_{gly}{}^{a}P_{co_2}{}^{b} \quad (4)$$

where r is rate of reaction (mol $gcat^{-1}$ s^{-1}), k is the rate constant, P_{gly} is the partial pressure of glycerol (kPa), P_{CO2} is the partial pressure of carbon dioxide (kPa) while a and b are the order of reaction unique to the catalyst system. The reaction rate constant, k was expressed in Arrhenius form (cf. Equation (5)) to estimate the activation energy.

$$k = Ae^{(-Ea/RT)} \quad (5)$$

where A is pre-exponential constant factor, s^{-1}; Ea is activation energy, kJ mol^{-1}; T is reaction temperature (K) and R is the gas constant, 8.314 J mol^{-1} K^{-1}.

3. Results and Discussion

3.1. Brunauer-Emmett-Teller (BET)

Table 1 shows the density, BET surface area and cumulative pore volume of the catalysts with increasing Ni metal loading. Density measurement results generally agreed with Taylor [11] who reported that the density of cement clinker (CC) was between 3.15 to 3.2 g cm^{-3}. BET surface area of the 100% CC was relatively low (0.55 m^2 g^{-1}) in agreement with prior work by Chitra [12]. Low surface area of CC apparently related to the sintering effect of calcination at 1723 K in the cement kiln [13]. Significantly, Ni-doping has increased the BET specific surface area of the catalysts. This is a further testament of the successful deposition of Ni on the CC surface. The pore size of the 100% CC falls in the range of macroporous as observed from the physisorption isotherms (not shown). The isotherms displayed a shift towards mesoporous range with metal loadings. Therefore, this indicates the formation of new compound attributed to the alteration of the surface structure of the catalysts, which was further confirmed by XRF analysis tabulated in Table 2.

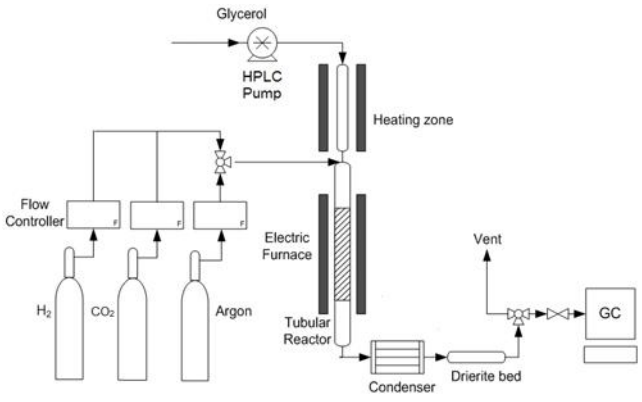

Figure 1. Experimental Setup

3.2 X-ray Fluorescence (XRF)

Table 2 shows that pure CC was in fact a mixture of oxide metals with CaO as the major ingredient at 61.98%. This also corresponds to the earlier studies by Kurdowski [9] and Tsakiridris *et al.* [10]. Further inspection of Table 2 also revealed that the percentage of CaO and SiO_2 in catalysts decreased from 61.98 % to 38.66 % and 17.21% to 6.77 % respectively as Ni metal loading being increased. Indeed, the doping of Ni has increased the amount of NiO that originally also presents in the pure CC, contributed to a spike from 62 ppm to 34.83%. This observation was also confirmed by XRD analysis (cf. Figure 2).

3.3. X-ray Diffraction (XRD)

XRD analysis was carried out for both CC (Reference) and Ni-loaded catalysts. Diffractograms were shown in Figure 2. The main mineralogical phase presents in the CC was alite (tricalcium silicate, Ca_3SiO_5) in agreement with Shih *et al.* [14] judging from 11 peaks shown in Figure 2. Alite found in CC presents as monoclinic crystals due to the impurity contents [15], differed from pure alite that is triclinic. XRD also confirmed the presence of calcium aluminum iron manganese oxide ($Ca_2Al_{0.}67Mn_{0.33}FeO_5$) in CC with orthorhombic shape.

For 5% Ni loading, clinker phase was essentially the same with presence of a substituted alite in nature named Hatrurite ($Ca_3O(SiO_4)$) [11]. Hatrurite has hexagonal crystals and X-ray lines were overlapped by those of larnite at 32.30°, 32.60°, 34.45°, 43.43°, 46.91° and 51.95° in consensus with findings by Gross [15]. Ni was bonded with free Mg and MnO to form nickel magnesium manganese oxide ($Ni_{0.9}MgO\text{-}_{0.1})_6MnO_8$ determined at peaks 18.20°, 43.43°, 46.91° and 60.08°. Moreover, calcium magnesium aluminum oxide ($Ca_{54}MgAl_2Si_{16}O_{90}$) species presence as orthorhombic (2θ = 29.53°,

32.30°, 32.60°, 34.45°, 41.31°, 51.95°, 56.54° and 62.35°) as evinced in 5% Ni-95% CC catalyst. Nonetheless, the peak intensities decreased with Ni content as compared with XRD patterns of 100% CC. This corroborated with Shui *et al.* [16] who reported that alite peaks ceases in fly ash and slowly replaced by $Ca_{54}MgAl_2Si_{16}O_{90}$ (flue gas desulfurater) after reactions. The crystal, $Ca_{54}MgAl_2Si_{16}O_{90}$ which acts as flue gas desulfurater was estimated to reduce the poisoning effect of catalyst during the reactions testing and enhance the catalytic performance.

For 10% Ni loading, calcium nickel catenadisilicate (Nickeldiopside, $CaNi(Si_2O_6)$) and calcium nickel silicate ($CaNiSi_4O_{10}$) was found in monoclinic and tetragonal system respectively. The presence of $CaNi(Si_2O_6)$ and $CaNiSi_4O_{10}$ were due to the existence of Ni, Ca_3SiO_5, silicon dioxide (SiO_2) and NiO, which underwent reactions in Eqs. (6) and (7) during the calcination stage as mentioned by Masse [17].

$$Ca_3SiO_5 + 5\ SiO_2 + 3\ NiO \rightarrow 3CaNiSi_2O_6 \quad (6)$$

$$Ca_3SiO_5 + 11\ SiO_2 + 3\ NiO \rightarrow 3CaNiSi_4O_{10} \quad (7)$$

For Ni loading more than 10%, the promotion of alite to larnite (ß-belite, Ca_2SiO_4) was being observed. Similar result was reported before by Sinyoung *et al.* [18]. They have investigated the effect of chromium metal loading in CC. Increasing peak intensities across 2θ of 37° and 43° signified the increment of crystalline size of larnite with Ni content.

In contrast, with Ni loading of up to 15%, Bunsenite (NiO), in cubic system and Ca_2SiO_4, in monoclinic were found to be the main components. The XRD results detected the crystalline in the form of Ca_2SiO_4 instead of Shannonite (γ-belite) which can be attributed to the presence of impurity ions and also slow rate of cooling after the calcination [10]. The results demonstrated that the Ni metal has inhibited the transformation of Ca_2SiO_4 back to Ca_3SiO_5 and there was no alite corresponding to results by Sinyoung *et al.* [18]. High Ni loading > 10% seems to assist the Ca_3SiO_5 polymorph to decompose and transform to Ca_2SiO_4, and NiO species as illustrated in Figure 2, as also obtained by Shih *et al.* [14].

With the loading of Ni metals, a slight shift of 2θ to a lower degree value can be observed from a closer scrutiny towards peaks occurs at 32° and 34° in Figure 3. Significant reduction of peaks intensities between 32-36° and left shifting effects indicates structural transformation due to Ni loading. Subsequently, the peak intensities especially the larnite compounds at peak 43° increases indicating an increase of crystalline size (cf. Figure 4 and Table 3). The XRD results (shows the occurrence of Bunsenite, NiO) are comparable with the results in XRF indicating a decreasing amount of CaO and SiO_2 for NiO formation.

Table 1. Composition, BET specific surface area and density of the catalysts

Composition (wt %)		BET specific surface area ($m^2\ g^{-1}$)	Density ($g\ cm^{-3}$)	Cumulative Pore Volume ($cm^3\ g^{-1}$)
Ni	CC			
0	100	0.55	2.99	0.0000
5	95	7.73	3.03	0.0022
10	90	15.81	3.12	0.0053
15	85	17.30	3.12	0.0054
20	80	17.83	3.22	0.0057

Table 2. XRF results of the catalysts

Catalysts	CaO	NiO	SiO_2	Al_2O_3	Fe_2O_3
100% CC	61.98	62*	17.21	3.90	3.53
5% Ni-95%CC	53.05	18.67	11.49	2.66	2.64
10% Ni-90%CC	57.02	14.14	8.44	3.07	3.16
15% Ni-85%CC	44.11	27.63	9.28	1.75	2.38
20% Ni-80%CC	38.66	34.83	6.77	1.36	2.07

*The data presented was in wt % except for * in ppm.*

3.4 FESEM Studies

The surface morphology obtained by FESEM imaging shows that the surface of pure CC (cf. Figure 5(a)) was very smooth and appeared non-porous. Interestingly, at the loading of 15% Ni (representative sample), the surface of the resulting catalyst has become rougher and bulkier with creation of more finely dispersed crystallites (cf. Fig. 5(b)). This may have explained the higher BET surface area obtained (cf. Table 1).

3.5 TGA- Calcination Studies

Calcination profiles of both 15% and 20% Ni doping in N_2 atmosphere was plotted as in Figure 6. Calcination profiles obtained from thermogravimetric analysis (TGA) shown in Figure 6 for pure 100% CC shows a thermal stability with no obvious decomposition. Calcination profiles for 15% Ni-85% CC and 20% Ni-80% CC catalysts (as representative samples) showed approximately similar trend of decomposition in N_2 atmosphere. Peaks formation before 500 K were probably due to the water vapour entrainment in the catalysts.

For both 15% and 20% Ni catalysts in Figure 6, there were formations of two peaks around 504 to 620 K and 620 to 794 K (with a shoulder peak around 673 K) respectively. The peaks for 20% Ni catalyst were shifted to the right as compared to 15% Ni catalyst. The first peak (504 to 620 K) was due to the transformation of $Ni_3(NO_3)_2(OH)_4$ to NiO in consensus with Estellé *et al*. [19]. It was also proven by the formation of highest peak that occurs at 580 K (green line) which indicates the full decomposition of nitrate in of nickel (II) nitrate hexahydrate ($Ni(NO_3)_2.6H_2O$) (cf. Figure 6). $Ni_3(NO_3)_2(OH)_4$ species was most likely obtained from the subsequent decomposition of $Ni(NO_3)_2.6H_2O$ during the drying of wet-impregnated catalyst at 403 K whilst second peak formed (620 to 794 K) was an indicative of NiO formation due to the total metal precursor (nickel (II) nitrate hexahydrate) decomposition in agreement with Loaiza-Gil *et al*. [20]. The calcination profiles corroborated with the XRD patterns which showed the presence of NiO. The formation of the shoulder peak at 673 K indicates the continuous thermal decomposition of a complex mixture of hydrated sili-

Table 3. Crystalline size of larnite, Ca_2SiO_4 at 2θ around 43° with Ni content

Ni loading	5%	15%	20%
2θ, degree	43.43	43.29	43.36
FWHM (β), degree	0.52	0.50	0.48
Crystalline Size (d), Å	172	179	186

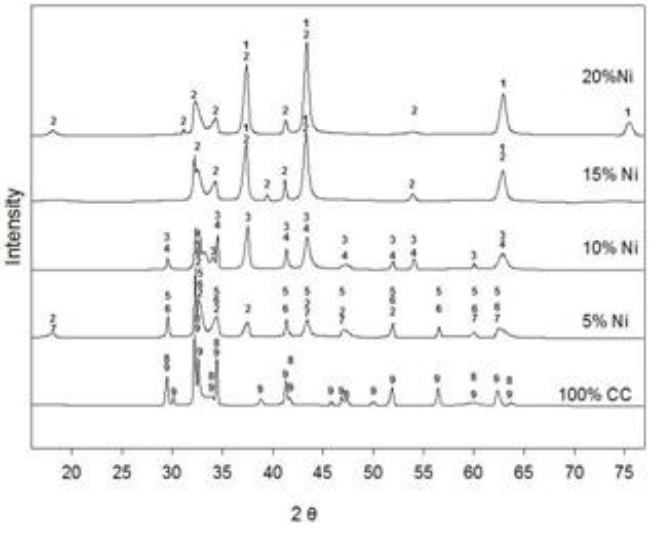

Figure 2. XRD results of catalysts. (1: Bunsenite, NiO; 2: Larnite, Ca_2SiO_4; 3: Calcium Nickel Catena Silicate, $CaNiSi_2O_6$; 4: Calcium Nickel Silicate, $CaNiSi_4O_{10}$; 5: Hatrurite, $Ca_3O(SiO_4)$; 6: Calcium Magnesium Aluminum Oxide Silicate, $Ca_{54}MgAl_2Si_{16}O_{90}$; 7: Nickel Magnesium Manganese Oxide, $(Ni_{0.9}MgO_{0.1})_6MnO_8$; 8: Calcium Aluminum Iron Manganese Oxide, $Ca_2Al_{0.67}Mn_{0.33}FeO_5$; 9: Alite, Ca_3SiO_5)

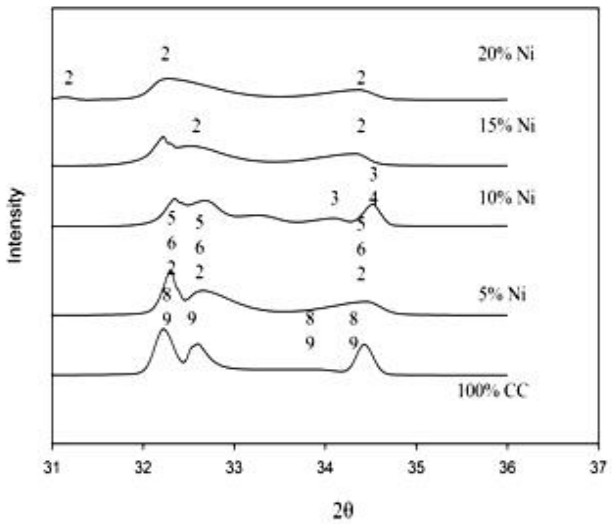

Figure 3. A closer scrutiny to compounds at 2θ of 31° to 36° (2: Larnite, Ca_2SiO_4; 3: Calcium Nickel Catena Silicate, $CaNiSi_2O_6$; 4: Calcium Nickel Silicate, $CaNiSi_4O_{10}$; 5: Hatrurite, $Ca_3O(SiO_4)$; 6: Calcium Magnesium Aluminum Oxide Silicate, $Ca_{54}MgAl_2Si_{16}O_{90}$; 8: Calcium Aluminum Iron Manganese Oxide, $Ca_2Al_{0.67}Mn_{0.33}FeO_5$; 9: Alite, Ca_3SiO_5)

cate and aluminate-type compounds as described by Gabrovšek *et al.* [21]. The decomposition of silicate described the formation of Ca_2SiO_4 crystalline present in 15% Ni-85% CC and 20% Ni-80% CC catalysts.

3.6 Reaction Studies

Figure 7 shows the hydrogen product ratio profiles for glycerol dry reforming carried out at 1023 K over 15%Ni-85% CC catalyst. Overall, H_2, CO and CH_4 were produced. Blank tests using the same feed with either an empty reactor or 100% CC bed yielded negligible glycerol conversion. This suggests that neither homogeneous gas phase glycerol dry reforming nor reaction over sites on the support occurred at detectable rates. The slight decrease of H_2:CO ratio with P_{CO2} is most likely an attribute of the reverse-water-gas-shift reaction. Nonetheless, the H_2:CO ratio remained > 1.0. In addition, the formation behaviour of both CH_4 and CO also forms the focal point of the current study as these two species are well-known carbon precursors via methane cracking and Boudouard reaction respectively. Hence, transient product ratio profiles of CO:CH_4 were plotted and shown in Figure 8 for 15% Ni-85% CC catalyst at different partial

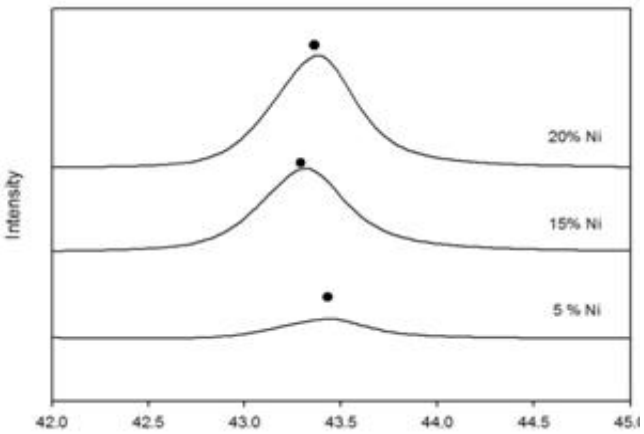

Figure 4. Peaks intensities of larnite, Ca_2SiO_4 at 2θ around 43° with Ni content

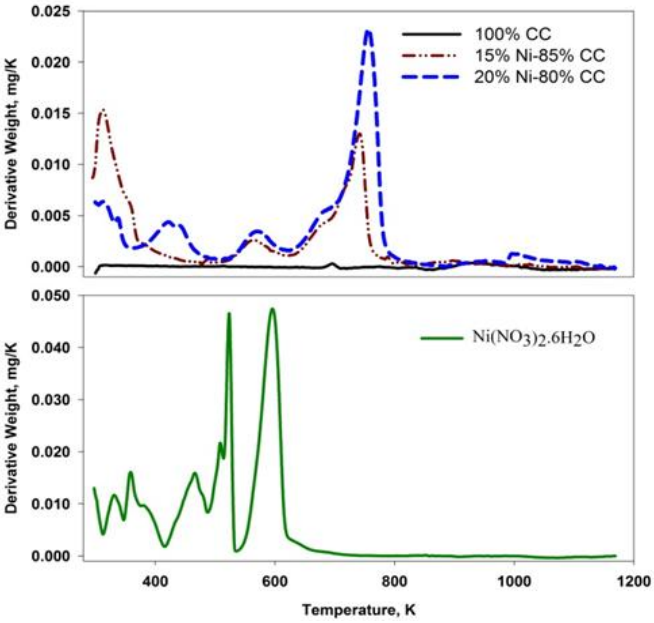

Figure 6. TGA analysis of catalysts and $Ni(NO_3)_2.6H_2O$ at 10 K min^{-1} ramping rate in N_2 atmosphere

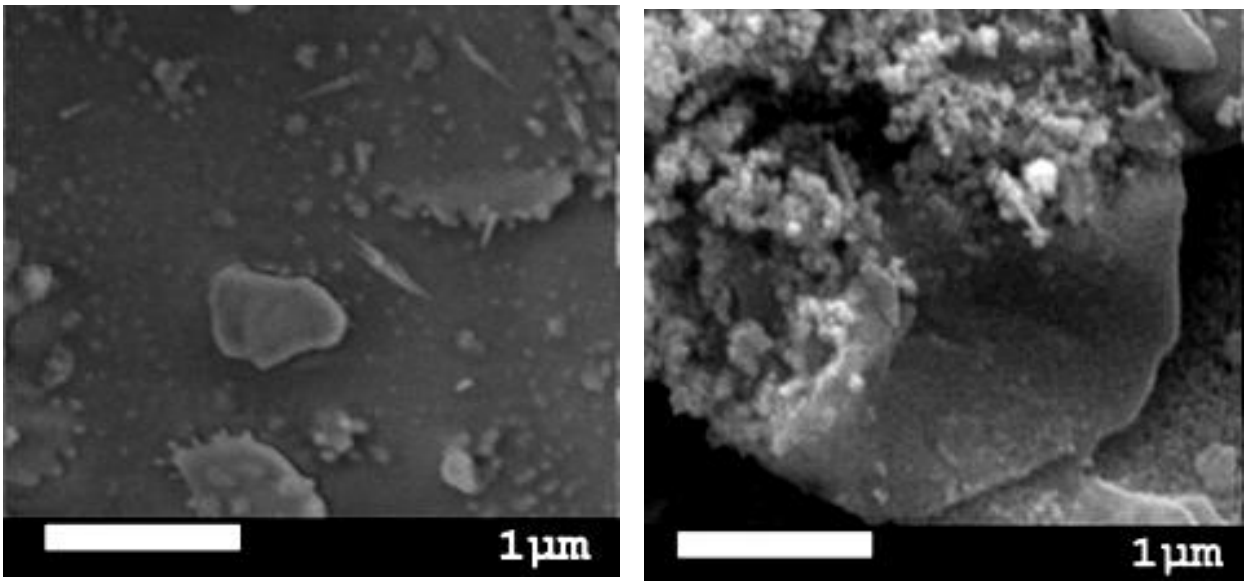

Figure 5. FESEM image, (a) fresh CC support and (b) fresh 15% Ni-85% CC

pressure of carbon dioxide, P_{CO2}. For P_{CO2} at 42 kPa (CGR 3:1), the CO:CH_4 ratio increased in the first 30 min of reaction time and thereafter gradually dropped. For P_{CO2} at 14.0 kPa (CGR 1:1), the CO:CH_4 ratio gradually increases up to 6.5, an indication of the decrease in CH_4. Indeed, higher CGR and higher temperature favour the formation of CO. However, Figure 8 depicts that the CH_4 formation was also increased with higher CGR. This could be explained by Equation (8), where the excess CO_2 has reacted with H_2 to form methane, CH_4. This was further proven by the methane production rate illustrated in Figure 9. The average methane production rate for 15% Ni-85% CC catalysts at P_{CO2}, 14.0 kPa (CGR 1:1) was 1.46E-5 mol g_{cat}^{-1} s^{-1} while for the P_{CO2} of 42.0 kPa, with CGR 3:1, the average methane production rate was 4.9E-5 mol g_{cat}^{-1} s^{-1}.

$$CO_2 + 4H_2 \leftrightarrow CH_4 + 2H_2O \quad (8)$$

Interestingly, excess CO_2 (culminate in CGR 3:1) did not promote Boudouard reaction (cf. Equation (9) to form CO as the CO to CH_4 ratio remained constant at circa 4.6 for CGR 3:1 (P_{CO2}= 42.0 kPa). Most likely, reaction as in Eq. (10) also has taken place.

$$2CO \leftrightarrow CO_2 + C \quad (9)$$

$$CO_2 + 2H_2 \leftrightarrow C + 2H_2O \quad (10)$$

Therefore, P_{CO2} needed to be regulated to obtain the maximum conversion of glycerol with the least carbon deposition.

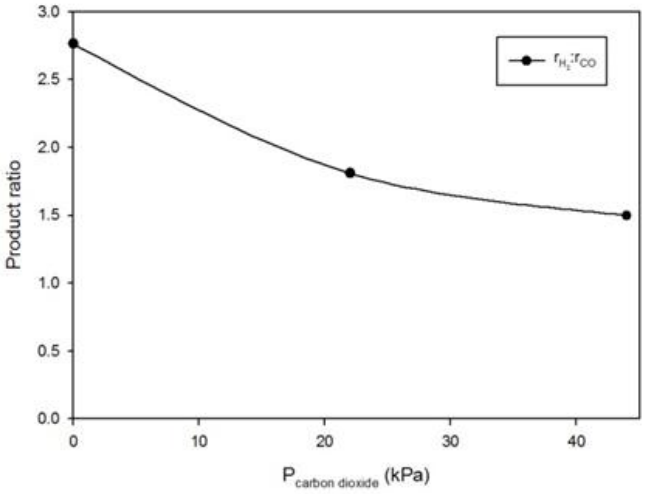

Figure 7. H_2:CO product ratio at 1023 K

4. Conclusion

Cement clinker catalyst with Ni dopants could be a potential catalyst for the purpose of producing syngas from glycerol dry reforming. Physicochemical characterization has revealed that cement clinker was a complex mixture of oxide compounds with CaO and SiO accounted for more than half (62% and 17% respectively). Although cement clinker was non-porous, addition of Ni has improved significantly the BET surface area with at least 32-folds increment. XRD examination showed formation of complex oxide phases depending on the Ni loading. Interestingly, glycerol dry reforming reaction yield H_2:CO < 2.0, suitable for

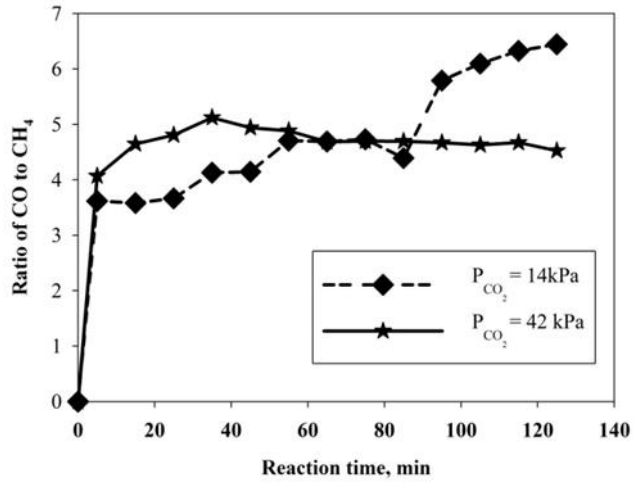

Figure 8. Typical transient CO:CH_4 of 15% Ni-85% CC catalysts for P_{CO2} = 14 kPa and P_{CO2} = 42 kPa at 1023 K

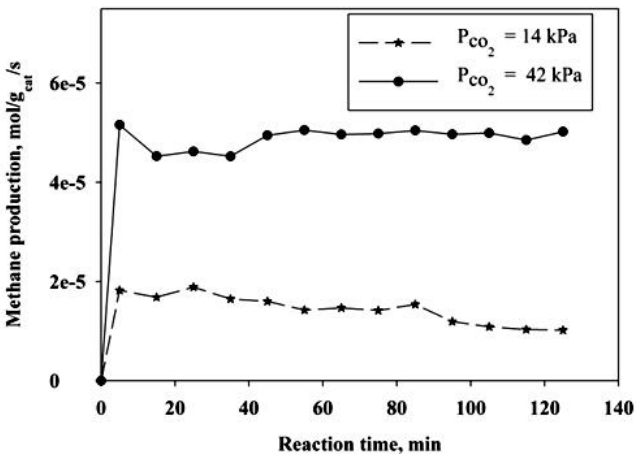

Figure 9. Methane production rate of 15% Ni-85% CC catalysts at P_{CO2} = 14 kPa and P_{CO2} = 42 kPa at 1023 K

Fischer-Tropsch synthesis. Nonetheless, the side-reactions such as methanation and hydrogenation of CO_2 have majorly affected the amount of syngas produced.

References

[1] Rossi, D.M., Costa, J. B., Souza, E.A., Peralba, M.C.R., Samios, D., Ayub, M.A.Z. (2011). Comparison of Different Pretreatment Methods for Hydrogen Production using Environmental Microbial Consortia on Residual Glycerol from Biodiesel. *International Journal of Hydrogen Energy* 36: 4814-4819.

[2] Wang, X., Li, M., Wang, M., Wang, H., Li, S., Wang, S., Ma, X. (2009). Thermodynamic Analysis of Glycerol Dry Reforming of Hydrogen and Synthesis Gas Production. *Fuel* 88: 2148-2153.

[3] Dantas, S.C., Escritori, J.C., Soeres, R.R., Hori, C.E. (2010). Effect of Different Promoters on $Ni/CeZrO_2$ Catalyst for Autothermal Reforming and Partial Oxidation of Methane. *Chemical Engineering Journal,* 156: 380-387.

[4] Bermúdez, J.M., Fidalgo, B., Arenillas, A., Menéndez, J.A. (2012). CO_2 Reforming of Coke Oven Gas over A $Ni/\gamma Al_2O_3$ Catalyst to Produce Syngas for Methanol Synthesis. *Fuel* 94: 197-203.

[5] Zhang, Y., Zhang, G., Zhang, B., Guo, F., Sun, Y. (2011). Effects of Pressure on CO_2 Reforming of CH_4 over Carbonaceous Catalyst. *Chemical Engineering Journal* 173: 592-597.

[6] Bellido, J.D.A., Souza, J.E.D., M'Peko, J.C., Assaf. E.M. (2009). Effect of Adding CaO to ZrO_2 Support on Nickel Catalyst Activity in Dry Reforming of Methane. *Applied Catalysis A: General* 358: 215-223.

[7] Al-fatish, A.S.A., Ibrahim, A.A., Fakeeha, A.H., Soliman, M.A., Siddiqui, M.R.H., Abasaeed, A.E. (2009). Coke Formation during CO_2 Reforming of CH_4 over Alumina-supported Nickel Catalysts. *Applied Catalysis A: General* 364: 150-155.

[8] Ruckenstein, E., Hu, Y.H. (1995). Carbon Dioxide Reforming of Methane over Nickel/Alkaline Earth Metal Oxide Catalysts. *Applied Catalysis A: General* 133: 149-161.

[9] Kurdowski, W. (2002). Role of Delayed Release of Sulphates from Clinker in DEF. *Cement and Concrete Research* 32: 401-407.

[10] Tsakiridis, P.E., Agatzini-Leonardaou, S., Oustadakis, P., Katsioti, M., Mauridou, E. (2005). Examination of The Jarosite-Alunite Precipitate Addition in The Raw Meal for The Production of Portland Cement Clinker. *Cement and Concrete Research* 35: 2066-2073.

[11] Taylor, H.F.W (1997). *Cement Chemistry*, London: Thomas Telford Publishing. 89.

[12] Chitra, C. (2011). Biodiesel Production from Rubber Seed Oil using Activated Clinker as Catalyst. *Bachelor Degree Thesis*, Universiti Malaysia Pahang.

[13] Li, H., Agrawal, D.K., Cheng, J., Silsbee, M.R. (1999). Formation and Hydration of C_3S Prepared by Microwave and Conventional Sintering. *Cement and Concrete Research* 29: 1611-1617.

[14] Shih, P., Chang, J., Lu, H., Chiang, L. (2005). Reuse of Heavy Metal-containing Sludges in Cement Production. *Cement and Concrete Research* 35: 2110-2115.

[15] Gross, S. (1997). The Mineralogy of The Hatrurim Formation, Israel. *Geol. Survey Israel Bull., 70*: 80.

[16] Shui, A., Gong, H., Zeng, L., Wang, H., Liu, P., Cheng, X. (2008). Preparation of Flue Gas Desulfurater by Mechanochemical Effect. *Bulletin of The Chinese Ceramic Society* 27(1): 1001-1625.

[17] Masse, S., Boch, P., Vaissière, N. (1999). Trapping of Nickel and Cobalt in $CaNiSi_2O_6$ and $CaCoSi_2O_6$ Diopside-Like Phases in Heat-Treated Cement. *Journal of European Ceramic Society* 19: 93-98.

[18] Sinyoung, S., Songsiriritthigul, P., Suwimol, A., Kajitvichyanukul, P. (2011). Chromium Behavior during Cement-Production Processes: A Clinkerization, Hydration, and Leaching study. *Journal of Hazardous Materials* 191: 296-305.

[19] Estellé, J., Salagre, P., Cesteros, Y., Serra, M., Medina, F., Sueiras, J.E. (2003). Comparative Study of The Morphology and Surface Properties of Nickel Oxide Prepared from Different Precursors. *Solid State Ionics* 156: 233-243.

[20] Loaiza-Gil, A., Villarroel, M., Balbuena, J.F., Lacruz, M.A., Gonzalez-Cortés. (2008). Thermal Decomposition Study of Silica-supported Nickel Catalyst Synthesized by The Ammonia Method. *Journal of Molecular Catalysis A: Chemical* 281: 207-213.

[21] Gabrovšek, R., Vuk, T., Kaučič, V. (2006). Evaluation of the Hydration of Portland Cement Containing Various Carbonates by Means of Thermal Analysis. *Acta Chim. Slov.* 53: 159-165.